# Defect Detection Using Regression Analysis of Transient Signal Data

James F. Plusquellic*, Donald M. Chiarulli@ and Steven P. Levitan+
*Department of CSEE, University of Maryland, Baltimore County
@Department of Computer Science, University of Pittsburgh
+Department of Electrical Engineering, University of Pittsburgh

## Abstract

*Transient Signal Analysis is a digital device testing method that is based on the analysis of voltage transients at multiple test points and on $I_{DD}$ switching transients on the supply rails. We show that it is possible to identify defective devices by analyzing the transient signals measured at test points on paths not sensitized from the defect site. The small signal variations generated at these test points are analyzed in both the time and frequency domain. Linear regression analysis is used to show the presence of correlation in these signals across the outputs of defect-free devices. However, there is a definite lack of correlation between output signals of defective devices with bridging and open drain defects. We present an automatic procedure based on the mean and standard deviation of regression residuals that is able to distinguish between defect-free and defective devices.*

## 1.0 Introduction

Transient Signal Analysis (TSA) [1] is a parametric approach to testing digital integrated circuits. Defect detection is accomplished in TSA by analyzing the transient signals of a device measured simultaneously at multiple test points. The approach offers two distinct advantages over other logic and parametric testing methods. First, device coupling mechanisms permit the detection of defects at test points that are not on logic signal propagation paths from the defect site (off-path nodes) [2][3]. Consequently, direct observation of logic faults is not necessary in TSA. Second, the cross-correlation of multiple test point signals allows signal variations caused by process tolerances to be distinguished from those caused by defects. This is true because process tolerance effects tend to be global, causing signal changes on all test points of the device. In contrast, signal variations caused by a defect tend to be regional and more pronounced on test points closest to the defect site [4].

In this paper, we focus on the development of a statistical method that can be used to automate the TSA testing process. We introduce Signature Waveforms (SWs) as a means of capturing signal variations between defect-free and defective devices and formulate two statistics based on a compact representation

of the SWs called Trapezoidal Rule Areas (TRAs). We evaluate the effectiveness of the TRAs in capturing the signal variations observable in the SWs separately in the time and frequency domain. The evaluation is performed by analyzing the TRAs from test point pairing of defect-free and defective devices using linear regression. The regression line computed for each pairing of the TRAs of defect-free devices tracks the variations introduced by process tolerances. The deviations or residuals of the TRAs of defective devices are computed with respect to the regression lines and summarized in two statistics, the absolute mean and standard deviation. The statistics computed for defect-free and defective devices are compared to determine the effectiveness of the TRAs in capturing the signal variations introduced by defects.

The analysis is performed using the time, Fourier magnitude and phase SWs obtained from four hardware experiments. One experiment is used as a control experiment to evaluate error in the estimates of the regression lines. The results of the three remaining experiments show that the phase TRAs are consistent with the signal behavior observed in the SWs and are best able to capture the variations produced by defects. Based on these results, we propose an algorithm that can be used to automate the detection of defects and discuss other issues important to the further development of TSA as a device testing method.

The remainder of this paper is organized as follows. Section 2.0 provides background and the motivation for our research. In Section 3.0, we describe the hardware experiments and the defect types and locations. In Section 4.0, the TSA testing method is described. Section 5.0 presents an analysis of regression line estimation error. In Section 6.0, we evaluate the effectiveness of the different TRAs representations in capturing the signal variations of defects. Section 7.0 presents a summary and conclusions.

## 2.0 Background and Motivation

Parametric device testing strategies [5][6] are based on the analysis of a circuit's parametric properties, for example, propagation delay, magnitude of quiescent supply current or transient response. Parametric methods have been shown to be more effective than conventional logic based methods in detecting common types of CMOS defects [7][8]. Many types of parametric tests have been proposed [9] but recent research interest has focused primarily on three types; $I_{DDQ}$ [10], $I_{DD}$ [11], and delay fault testing [12][13].

$I_{DDQ}$ is based on the measurement of an IC's supply current when all nodes have stabilized to a quiescent value [14]. $I_{DDQ}$ has been shown to be an effective diagnostic technique for CMOS bridging defects, but is not applicable to all types of CMOS defects [15]. Although defect observability is significantly

improved by the addition of $I_{DDQ}$ to logic tests, $I_{DDQ}$ is handicapped by the necessarily slow test vector application rates, the limited resolution achievable for large ICs and the restricted class of CMOS circuits to which it is applicable. Recently, concerns have been raised over the applicability of IDDQ to deep submicron technologies [16].

Several dynamic supply current $I_{DD}$-based approaches have since been proposed to overcome the limitations caused by the static nature of the $I_{DDQ}$ test [11][17][18][19][20]. In general, these $I_{DD}$-based methods are not hampered by the slow test application rates and are not as sensitive to design styles as $I_{DDQ}$, however, circuit size and topology are still factors that affect the defect resolution of these schemes. Also, these methods do not provide a means of accounting for process tolerances and are therefore subject to aliasing problems.

Alternatively, delay fault testing takes advantage of the fact that many CMOS defects cause a change in the propagation delay of signals along sensitized paths [8]. Since the test is dynamic and regional, delay fault testing does not suffer from slow test vector application rates, as is true of $I_{DDQ}$, and is not as sensitive to circuit size, like $I_{DD}$. One of the difficulties with delay fault testing is that test vector generation is complicated due to static and dynamic hazards [21]. Also, since the number of possible paths in a circuit is much larger than the number of paths that are typically tested, the effectiveness of a delay fault test is dependent on the propagation delay of the tested paths and the delay defect size, for path delay fault testing, and the accuracy of the test equipment, for gate delay fault testing [23]. Lastly, Pierzynska and Pilarski have shown that a non-robust test can detect a delay fault undetectable by any robust test [22]. Franco and McCluskey [24] and others [25][26][27] have proposed extensions to delay fault testing that address some of these difficulties.

Recently, Ma, *et al.* [28] and others [7][8][29][30] evaluated a large number of test methodologies and determined that a combination of several test strategies may be necessary in order to find all defective devices. In particular, Ma, *et al.* discovered that $I_{DDQ}$ cannot detect all kinds of defects and must be used with some kind of dynamic voltage test. Our technique, Transient Signal Analysis (TSA), with its advantages in defect detection and process insensitivity, is proposed as an addition to this test suite.

## 3.0 Experiment Summary

In this section, we present a summary of the experiment setup and show the types and locations of the

defects that we introduced into a set of test devices. We conducted hardware experiments on ICs with bridging and open drain defects. Of the four basic CMOS defect types--bridges, opens, gate oxide shorts and parametric defects--bridges have been selected due to their ubiquity and open drains have been selected because they represent one of the most difficult of CMOS defects to detect reliably.

The hardware experiments were conducted on three versions of the ISCAS85 c432 benchmark circuit: a version with intentionally inserted bridging defects, a version with intentionally inserted open drain defects and a defect-free version [31]. Four devices of each version were fabricated through MOSIS. The four defect-free devices and one set of either the open drain or bridging defective devices were used in each experiment. Four experiments were conducted, two bridging experiments labeled Internodal-Bridging and Feedback-Bridging, and two open drain experiments labeled Open-Drain and Control.

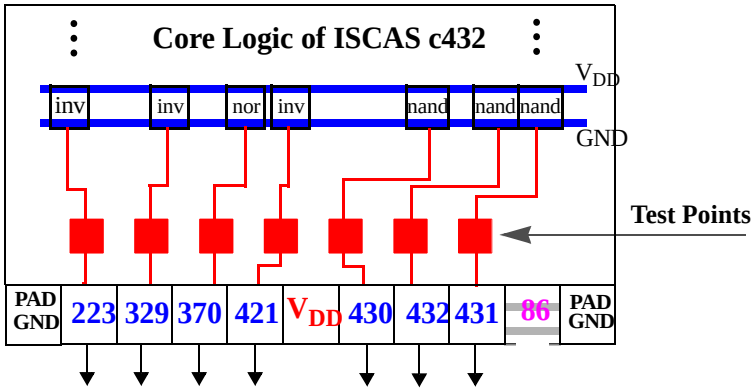


**Figure 1. Location of the test points on the c432.**

The primary outputs of the c432 are labeled 223 through 432 as shown along the bottom of Figure 1. The test points are twenty-two $\mu m^2$ metal-2 pads placed on the output nodes of the gates driving the seven primary outputs. The measurements were taken at a Karl Suss probe station using a PicoProbe, model 12C, with a 100 FF and 1 MΩ load. $I_{DD}$ was measured at the core logic $V_{DD}$ pin through a 10 Ohm resistor. A digitizing oscilloscope with a bandwidth of 1 GHz was used to collect a 2048 point waveform from each of the test points. The experiments were run at 11 MHz, about half the maximum operating frequency of the devices.

Figure 2 shows portions of the schematic diagram from the c432 for the bridging experiments. Only those sensitized paths affected by the defect are shown. The input stimulus for the Internodal Bridging experiment toggles PI 66. The dotted line in the figure represents the bridging defect which was created in the layout by inserting a first-level to second-level metal contact between the output lines of a 4-input

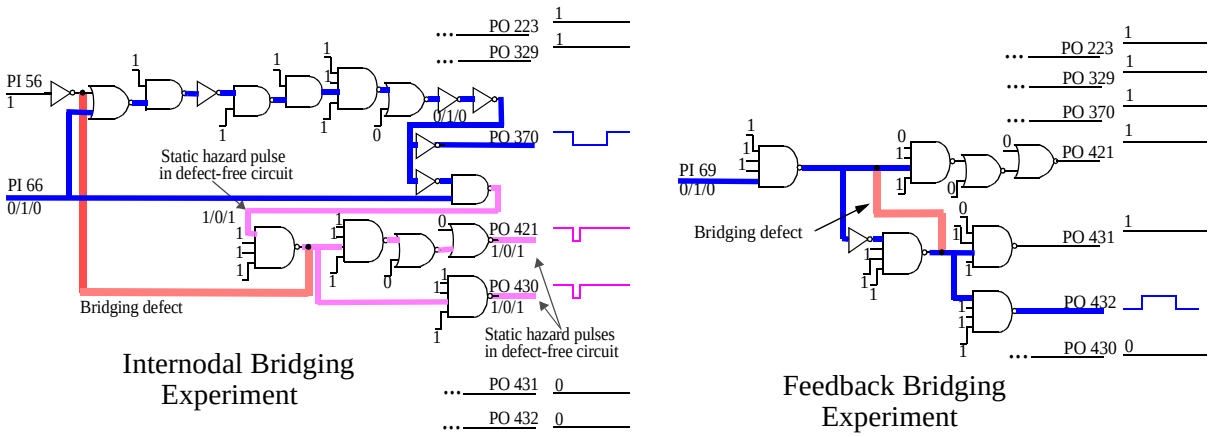


**Figure 2. Portions of the c432 showing the sensitized paths from the Bridging Experiments**

NAND gate and an inverter. In the defect-free devices, a static hazard causes a pulse to propagate to POs 421 and 430 along paths shown shaded in the figure. Since the output of the inverter driven by PI 56 is low, the bridge eliminates the pulse in the bridging defective devices. The left side of Figure 2 shows the sensitized paths for the Feedback Bridging experiment. Although the defect is on a sensitized path driving PO 432, the circuit operates logically correctly under this test sequence. The bridging defect is shown in the figure as a dotted line but is physically represented as an extra piece of second-level metal between the outputs of two 4-input NAND gates.

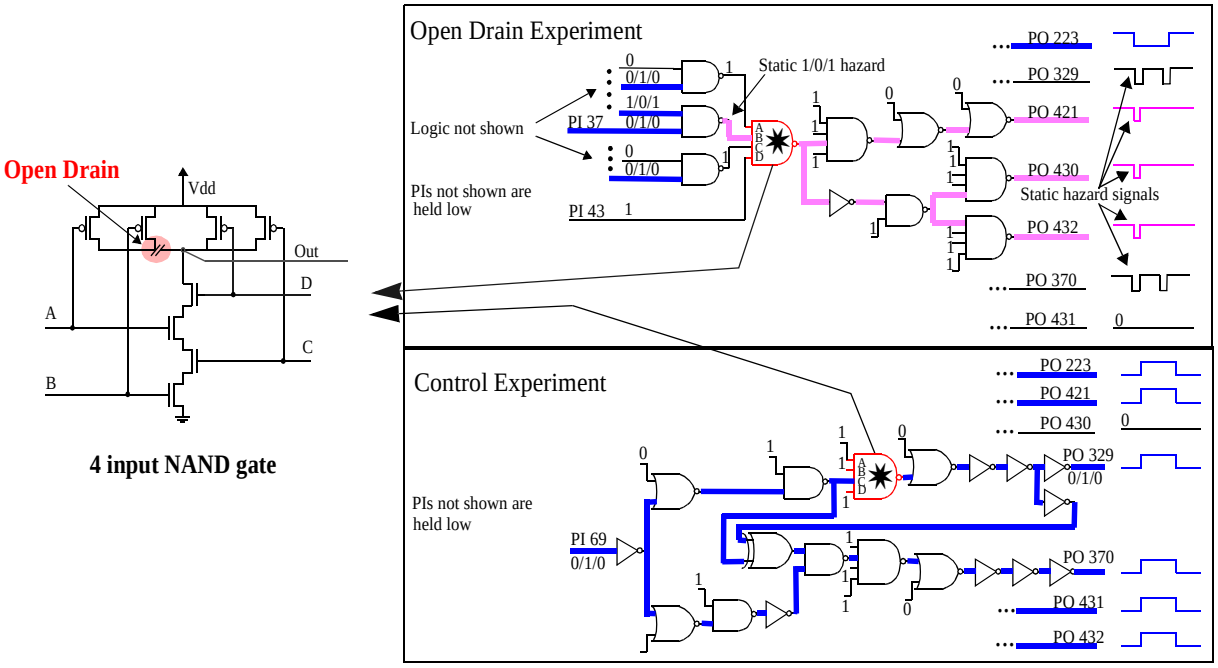


**Figure 3. Portions of the c432 showing the sensitized paths from the Open Drain and Control Experiments.**

Figure 3 shows the sensitized paths through the defective gates for the Open Drain (top) and Control

experiments (bottom). The left side of Figure 3 shows an open drain defect in the transistor-level schematic diagram of a 4-input NAND gate. A three micron wide piece of first-level metal has been removed between the p-transistor drain pairs. Both of the open drain experiments test this type of defect in two different NAND gates in the circuit. The test sequence for the Open-Drain experiment generates a number of pulses which are created by a static hazard in the defect-free devices but eliminated by the defect in the open drain devices. The Control experiment was designed to test the change in loading capacitance introduced by the defect on POs 329 and 370. The open drain, in this case, removes approximately 19% of the total output load capacitance.

| Experiment | Device Set 1 | Device Set 2 | Test sequence elicits a parametric fault in Device Set 2 |
|---|---|---|---|
| **Control** | 4 DF | 4 OD | No |
| **Internodal-Bridging** | 4 DF | 4 BR | Yes |
| **Feedback-Bridging** | 4 DF | 4 BR | Yes |
| **Open-Drain** | 4 DF | 4 OD | Yes |

**Table 1: Logic behavior of defective devices in the four experiments.**

Table 1 enumerates the four experiments that were conducted on the c432. The second and third columns indicate the number and identity of the devices with DF indicating Defect-Free, OD indicating Open-Drain and BR indicating BRidging. The last column indicates whether or not a change in parametric behavior is measurable among the devices of Device Set 2 under the test sequence. As noted in the table, the test sequence for the Control experiment does not produce measurable changes in parametric behavior of the Open-Drain devices. Since the Open-Drain devices behave like defect-free devices under these conditions, we use this experiment as a control experiment to evaluate the error in the regression line estimates. We later show that these same Open-Drain devices can be identified as defective when tested using an input stimulus that causes a fault (Open-Drain experiment).

Since the emphasis of these experiments is on the measuring the coupled variations introduced by the parametric faults at the test points, we analyze only the transient signals of test points that are not directly affected by parametric faults. For example, with respect to Figures 2 and 3, we analyze the signals of test points 223, 329, 370, 431, 432 and $I_{DD}$ of the Internodal-Bridging experiment, test points 223, 329, 370, 421, 430, 431 and $I_{DD}$ of the Feedback-Bridging experiment and test points 223, 329, 370, 431 and $I_{DD}$ of

both the Open Drain and Control experiments. We restricted the test points in the Control experiment to those analyzed in the Open Drain experiment in order to reduce undesirable sources of variation between the results of these experiments. We discuss this further in Section 5.0.

## 4.0 Testing Method

In this section, we describe the TSA testing method and the statistics used in the analysis. We introduce Signature Waveforms as a means of capturing signal variations between devices. A simple integration procedure is used to condense the information contained in Signature Waveforms into a single value called a Trapezoidal Rule Area or TRA. We then define standardized residuals in the context of scatter plots and develop a defect detection criteria using the mean and standard deviation of standardized residuals.

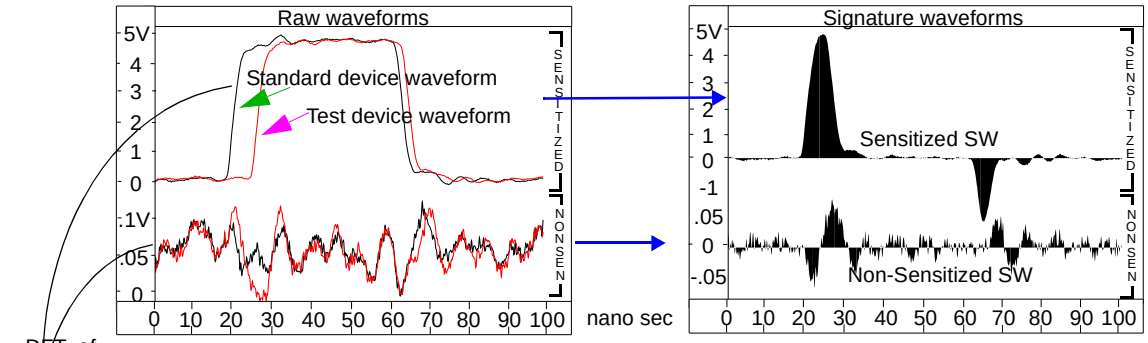


**Figure 4. Time Domain Signature Waveforms.**

**Figure 5. Frequency Domain Signature Waveforms.**

We use **Signature Waveforms** or **SWs** to capture signals variations between devices as shown in Figure 4. The plot labeled “Raw Waveforms” depicts the transient waveforms of two devices. The waveforms shown along the top of the plot were measured on test points that were driven by a sensitized path. The waveforms shown along the bottom were measured on non-sensitized test points. We create Time Domain Signature Waveforms from these pairs of transient waveforms by subtracting the test device waveform from the standard device waveform. The difference waveforms, shown in the right plot of Figure 4, are

shaded along a zero baseline in order to emphasize the signal variations.

The Sensitized SW, shown in the right plot of Figure 4, accurately captures propagation delay differences between the Standard and Test devices while the Non-Sensitized SW illustrates that significant signal variation occurs on non-sensitized test points as well. However, the time domain Signature Waveforms do not allow individual frequency component variations to be examined. Therefore, we also analyze the frequency domain representation of the transient signals by creating frequency domain Signature Waveforms as shown Figure 5. The magnitude and phase components produced by a Discrete Fourier Transform of the raw time domain waveforms are shown as waveforms in the left plot. Magnitude and Phase SWs on the right are created by subtracting the test device magnitude and phase values from the corresponding values of the standard device.

In order to simplify waveform post-processing, we compress the multi-point SWs into a single floating point value by computing the area under their curves using a Trapezoidal Rule integration method. We call the area value result a TRA. We recognize that the compaction process can result in waveform aliasing. Aliasing occurs when two or more SWs with different temporal or spectral attributes produce the same TRA. In TSA, we reduce the impact of this problem by using distribution moments of multiple test points TRAs as the defect detection criteria as described below.

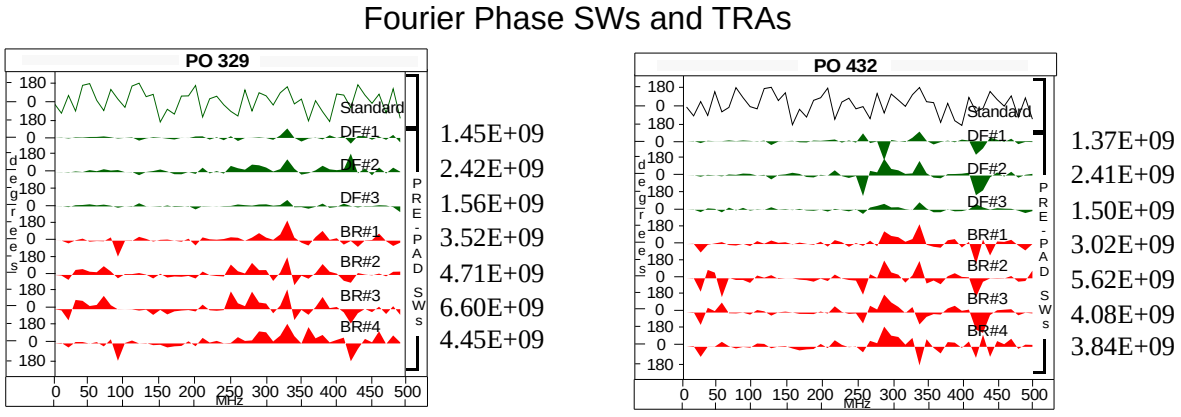


**Figure 6. Example Fourier Phase SWs and TRAs from test points 329 and 432.**

Figure 6 shows the Fourier Phase SWs from two non-sensitized test points, 329 and 432, of an hardware experiment involving one standard and seven test devices. The top-most waveform is the output trace of a defect-free device that is used as the standard. The SWs of three additional defect-free devices are labeled DF#*x* while the SWs of four BRidging defective devices are labeled BR#*x*. The TRAs shown to the right of each plot are computed over the portion of the frequency range between 10 to 250 MHz.

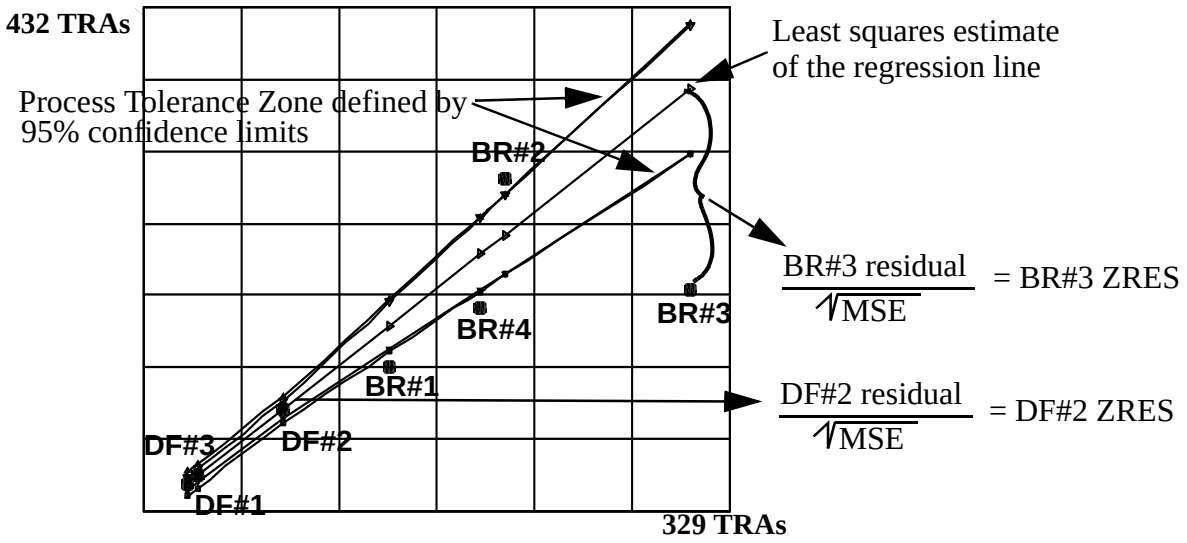


**Figure 7. Example Scatter Plot, Least Squares Estimate of the Regression Line and Standardized residuals (ZRES) for TRA pairing of test points 329 and 432.**

The statistics that we use to detect defects are based on standardized residuals. Standardized residuals are derived from two dimensional scatter plots of TRAs. For example, Figure 7 depicts a scatter plot derived from test points 329 and 432. The x and y values of the data points are given by the two columns of TRAs shown in Figure 6. We compute a least squares estimate of the regression line, $Y = b_0 + b_1 X$, through the defect-free data points, DF#1, DF#2 and DF#3. The parameters $b_0$ and $b_1$ of the regression line are estimated by the expressions

$$b_1 = \frac{\sum (x_i - \bar{x})(y_i - \bar{y})}{\sum (x_i - \bar{x})^2}$$

$$b_0 = \bar{y} - b_1 \bar{x}.$$

Residuals are computed as the distance along the y axis between the data points and the regression line as shown for data points BR#3 and DF#2 in Figure 4. The residuals are standardized using the expression

$$\text{ZRES} = \frac{\text{residual}}{\sqrt{MSE}}$$

where MSE is defined as the mean square error or sample variance of the three DF#x residuals. The residuals the BR#x data points are also standardized using this value.

In [1][4], we show that a high degree of linear correlation exists among the data points of defect-free

devices. This is consistent with our observations that variations in SWs resulting from process tolerance effects occur in all test point signals. Therefore, the regression line tracks process tolerance effects and, in the absence of unmodeled random variables such as measurement noise and intra-device process tolerances, the data points of defect-free devices would be co-linear. Instead, the data points of defect-free devices are distributed around the regression line and define a region that we call the process tolerance zone, as shown by 95% confidence limits in Figure 7. It is in this region that we expect to find the data points of defect-free devices.

In contrast, we have observed that defects introduce additional variation in the SWs of defective devices that varies depending on the state and position of the test point with respect to the defect site. As shown in Figure 7, this causes the data points of defective devices to fall outside of the process tolerance zone. Therefore, the standardized residuals of defective devices capture uncorrelated variation that results from defects in addition to the variation common to all data points, namely, that due to measurement noise, intra-device process tolerances and error in the regression line estimate.

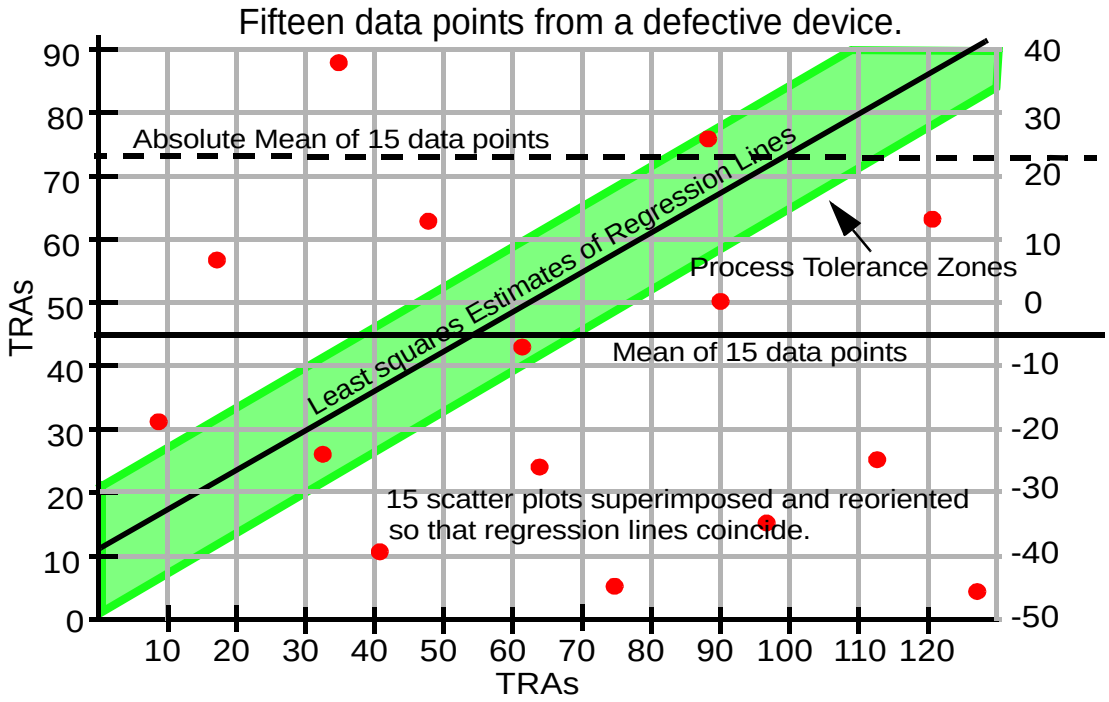


**Figure 8. Example of 15 superimposed scatter plots showing the mean and absolute mean of the data points from a single defective device.**

Our defect detection criteria is based on two statistics, the absolute mean, $|\mu|$, and standard deviation, $\sigma$, of standardized residuals. Figure 8 is a graphical illustration that aids in the visualization of these statistics. In this example, the transient signals from six test points are used in the analysis. Fifteen scatter plots

similar to the one shown in Figure 7 are derived using all pairings of the TRAs of the six test points. The fifteen scatter plots are shown superimposed in Figure 8 with all but the data points belonging to one device removed. The scatter plots have been reoriented in order to make the regression lines from the individual scatter plots coincide. |μ| is computed as the mean of the absolute value of the standardized residuals. σ is computed in the usual way using the mean of the standardized residuals. |μ| and σ measure the mean of the absolute deviation and the dispersion, respectively, of the data points around the regression lines. The analytical expressions for |μ| and σ are given as

$$|\mu| = \frac{1}{p} \sum_{\text{over all}}^{pairings} \left| \frac{Y - \hat{Y}}{\sqrt{MSE}} \right|$$

$$\sigma = \sqrt{\frac{1}{p-1} \sum_{\text{over all}}^{pairings} \left( \frac{Y - \hat{Y}}{\sqrt{MSE}} - \bar{Y} \right)^2}$$

where

$$\sqrt{MSE} = \sqrt{\sum_{i=1}^{3} \left( \frac{Y_{\text{defect-free}} - \hat{Y}}{n-2} \right)}$$

and

$$\bar{Y} = \frac{1}{p} \sum_{\text{over all}}^{pairings} \frac{Y - \hat{Y}}{\sqrt{MSE}}$$

$p$ = number of pairings

$\hat{Y}$ = regression line Y value at X

σ is a more powerful defect identification criteria when the signal variations caused by the defect are present in only a few test point signals. In this case, the non-robustness of the metric to outliers is a desirable property. |μ| is more robust to measurement error but less sensitive to defective device outliers.

| | **Experiment** | |
|---|---|---|
| **Device Id** | \|μ\| | σ |
| **BR#1** | 29.81 | 91.46 |
| **BR#2** | 42.82 | 78.37 |
| **BR#3** | 37.28 | 70.11 |
| **BR#4** | 21.26 | 27.94 |
| **$DF_{Max}$** | 0.82 | 0.80 |

**Table 2: Example** |μ| and σ **statistics table.**

Table 2 shows an example of a statistics table that we use to report results. The Device ID is given in

the left-most column while the second and third columns give the |μ| and σ statistics. The bottom row shows the maximum value computed for one of the three defect-free devices. By comparing the last row of values with the values in the rows above them, we can evaluate the significance of the difference between the defect-free devices and each of the defective devices. For example, the maximum |μ| and σ statistics of the defect-free devices are given as 0.82 and 0.80, respectively. The minimum |μ| and σ statistics are shown for BR#4 as 21.26 and 27.94 which are a factor of at least twenty larger than the maximum defect-free statistics. In the next section, we show that the |μ| and σ statistics of defective devices are significantly larger than those of defect-free devices and that the regression line estimates are reasonably approximated.

## 5.0 Regression Line Error Analysis

In this section, we estimate of the error in the regression lines using the |μ| and σ statistics of the Control experiment. The test sequence used in the Control experiment does not cause a logic fault in either the defect-free or defective devices and, therefore, the TRAs of both device sets capture only the signal variations of process tolerance effects and measurement noise. The regression lines are computed using the DF#x devices and the error evaluated by comparing the |μ| and σ OD#x statistics with the values computed for the DF#x devices. The analysis is performed separately using the time, magnitude and phase TRAs.

The expectation is that the |μ| and σ statistics of the OD#x devices will be larger than the DF#x statistics by an amount proportional to the error in the estimates of the regression lines. However, the significance of the error is difficult to evaluate without a context. We address this deficiency by presenting the results of the Open-Drain experiment as well. Since the test sequence used in the Open-Drain experiment causes a logic fault, the |μ| and σ statistics additionally capture the regional variation caused by the defect. Again, we expect the |μ| and σ statistics of the OD#x devices to be larger than the DF#x statistics. More important in this analysis, however, is the difference between the two sets of OD#x statistics under each test sequence. In this case, the error in the regression line estimates is present in both sets of statistics and can be compared in magnitude with the difference between the two sets of OD#x statistics.

| | Control Exp. | | Open-Drain Exp. | |
|---|---|---|---|---|
| **Device Id** | \|μ\| | σ | \|μ\| | σ |
| **OD#1** | 3.85 | **9.19** | 23.01 | 92.42 |
| **OD#2** | **4.04** | 7.89 | 10.85 | 33.67 |
| **OD#3** | 3.20 | 4.23 | **4.32** | **9.07** |
| **OD#4** | 2.58 | 3.53 | 10.95 | 37.13 |
| **$DF_{Max}$** | **0.79** | **0.57** | 0.64 | 0.55 |

**Table 3: Statistical results using Time Domain TRAs of test point pairings 329, 370, 431 and $I_{DD}$ for the Control and Open-Drain experiments.**

Table 3 shows the Time Domain |μ| and σ statistics of the Control and Open-Drain experiments computed using the TRAs of test points 329, 370, 431 and $I_{DD}$. The test sequence of the Open-Drain experiment causes a logic fault on test points 421, 430 and 432. Consequently, these test points are excluded in the analysis. 223 is also excluded because of measurement error, but is an important result of its own as discussed in [4].

The shaded cells shown along the bottom of columns two and three are the maximum of the three |μ| and σ statistics of the defect-free devices and are given as 0.79 and 0.57, respectively. The shaded |μ| and σ statistics of the OD#x devices in these columns are also the maximum values and are given as 4.04 and 9.19. This indicates that the OD |μ| statistic is larger than the DF value by a factor of 5.1 and the σ statistic is larger by a factor of 16.1. As discussed above, these statistics indirectly measure the error in the estimates of the regression lines.

Columns four and five of Table 3 shows the |μ| and σ statistics of the Open-Drain experiment. In these results, the minimum |μ| and σ statistics are shaded since we are interested in evaluating the worst case or the smallest difference between the two sets of OD#x statistics. The minimum values are given by device OD#3 as 4.32 and 9.07. The values obtained in the Control experiment of 4.04 and 9.19 make it difficult to identify the variation introduced by the defect in these results. This is true because the width of the region between the two sets of OD#x statistics is only 0.28 for |μ| and is less than zero for the σ. Therefore, the Time Domain analysis does not adequately distinguish between the signal behaviors caused by defects and

those caused by process tolerance effects.

| | Control Exp. | | Open-Drain Exp. | |
|---|---|---|---|---|
| **Device Id** | $\|\mu\|$ | $\sigma$ | $\|\mu\|$ | $\sigma$ |
| **OD#1** | 3.97 | 3.47 | 10.95 | 13.19 |
| **OD#2** | **7.31** | **7.33** | 38.84 | 76.99 |
| **OD#3** | 1.12 | 1.43 | **10.23** | **10.46** |
| **OD#4** | 4.61 | 4.42 | 12.58 | 14.46 |
| **$DF_{Max}$** | **0.74** | **0.82** | 0.70 | 0.74 |

**Table 4: Statistical results using Fourier Magnitude TRAs of test point pairings 329, 370, 431 and $I_{DD}$ for the Control and Open-Drain experiments.**

Table 4 shows the $|\mu|$ and $\sigma$ statistics computed using the Magnitude TRAs of the Control and Open-Drain experiments. The maximum Control $|\mu|$ and $\sigma$ statistics are 7.31 and 7.33, respectively, which is a factor of ten larger than the maximums computed for the defect-free devices. The minimum $|\mu|$ and $\sigma$ statistics shown shaded on the right side of Table 4 are 10.23 and 10.46. Although the region between the two sets of statistics is non-zero in both cases, the tolerance is less than half of the regression line error estimate. Similar to conclusions drawn from the Time Domain results, the Magnitude results do not adequately distinguish between the signal behaviors caused by defects and those caused by process tolerance effects.

| | Control Exp. | | Open-Drain Exp. | |
|---|---|---|---|---|
| **Device Id** | $\bar{\mu}$ | $\sigma$ | $\bar{\mu}$ | $\sigma$ |
| **OD#1** | 2.88 | 3.57 | **248.29** | **425.62** |
| **OD#2** | **3.29** | **4.21** | 272.43 | 434.79 |
| **OD#3** | 1.48 | 1.63 | 327.77 | 556.87 |
| **OD#4** | 2.96 | 3.01 | 306.71 | 514.93 |
| **$DF_{Max}$** | **0.75** | **0.18** | 0.73 | 0.80 |

**Table 5: Statistical results using Fourier Phase TRAs of test point pairings 329, 370, 431 and $I_{DD}$ for the Control and Open-Drain experiments.**

Table 5 shows the $|\mu|$ and $\sigma$ statistics computed using the Phase TRAs of the Control and Open-Drain experiments. The maximum OD#x $|\mu|$ and $\sigma$ statistics are 3.29 and 4.21, respectively. Although this factor is approximately five times the expected value of $|\mu|$ and twenty-five times the expected value of $\sigma$, the minimum $|\mu|$ and $\sigma$ statistics shown for the Open-Drain experiment are 248.29 and 425.62. These values are larger than OD#x statistics of the Control experiment by a factor greater than seventy-five. Therefore,

the Phase analysis is most useful in distinguishing between the two types of variations.

## 6.0 Defect Detection using Regression Analysis

In this section, we present the results of two additional experiments conducted on a second set of defective devices with intentionally inserted bridging defects. Since the |μ| and σ statistics are based on standardized residuals, a meaningful comparison of these results with the statistics computed in the previous section is possible. Again, we demonstrate that the phase TRAs are best able to capture the variations produced by defects. Based on the results of regression analysis, we propose an algorithm that can be used to automate TSA.

| \|μ\| | Experiment | | | |
|---|---|---|---|---|
| **Device** | **Control** | **Open-Drain** | **Internodal-Bridge** | **Feedback-Bridge** |
| **OD/BR#1** | 3.85 | 23.01 | 29.81 | 18.56 |
| **OD/BR#2** | **4.04** | 10.85 | 42.82 | **10.62** |
| **OD/BR#3** | 3.20 | **4.32** | 37.28 | 26.12 |
| **OD/BR#4** | 2.58 | 10.95 | **21.26** | 23.53 |
| **$DF_{Max}$** | 0.79 | 0.64 | 0.82 | 0.59 |

**Table 6: Summary of Time Domain |μ| Statistics.**

| σ | Experiment | | | |
|---|---|---|---|---|
| **Device** | **Control** | **Open-Drain** | **Internodal-Bridge** | **Feedback-Bridge** |
| **OD/BR#1** | **9.19** | 92.42 | 91.46 | 88.98 |
| **OD/BR#2** | 7.89 | 33.67 | 78.37 | **36.79** |
| **OD/BR#3** | 4.23 | **9.07** | 70.11 | 66.73 |
| **OD/BR#4** | 3.53 | 37.13 | **27.94** | 104.86 |
| **$DF_{Max}$** | 0.57 | 0.55 | 0.80 | 0.62 |

**Table 7: Summary of Time Domain σ Statistics.**

For convenience of reference, we repeat the |μ| and σ statistics computed for the Control and Open-Drain experiments in the previous section and present the |μ| and σ statistics in separate tables. Tables 6 and 7 show a summary of the Time Domain |μ| and σ statistics, respectively. The left-most column identifies the device with, OD indicating Open-Drain and BR indicating BRidging. The |μ| and σ statistics of each of the four experiments are shown in columns two through five. The shaded value in column two is the maximum among the defective device values while the shaded values in columns three, four and five

are the minimum values. The bottom row depicts the maximum Defect-Free |μ| and σ statistics for each experiment.

As indicated in columns four and five of Tables 6 and 7, the Time Domain |μ| and σ statistics computed for the BR#x devices are moderately larger on average than the values shown in column three for the OD#x devices. Moreover, the difference between the maximum OD#x statistics under the Control test sequence and the minimum BR#x statistics indicates that the Time Domain TRAs were able to capture some of the regional variation caused by the defect. For example, the maximum σ statistic in column 2 is 9.19 while the minimum σ statistics in columns four and five are 27.94 and 36.79 yielding differences of 18.75 and 27.60, a factor of at least two larger than the error in the regression line estimates.

| \|μ\| | Experiment | | | |
|---|---|---|---|---|
| **Device/Experiment** | **Control** | **Open-Drain** | **Internodal-Bridge** | **Feedback-Bridge** |
| **OD/BR#1** | 3.97 | 10.95 | **9.70** | 13.40 |
| **OD/BR#2** | **7.31** | 38.84 | 12.05 | **15.89** |
| **OD/BR#3** | 1.12 | **10.23** | 20.85 | 54.97 |
| **OD/BR#4** | 4.61 | 12.58 | 20.48 | 17.05 |
| **$DF_{Max}$** | 0.74 | 0.70 | 0.79 | 0.67 |

**Table 8: Summary of Magnitude |μ| Statistics.**

| σ | Experiment | | | |
|---|---|---|---|---|
| **Device/Experiment** | **Control** | **Open-Drain** | **Internodal-Bridge** | **Feedback-Bridge** |
| **OD/BR#1** | 3.47 | 13.19 | **13.00** | **45.70** |
| **OD/BR#2** | **7.33** | 76.99 | 20.88 | 53.69 |
| **OD/BR#3** | 1.43 | **10.46** | 42.20 | 205.75 |
| **OD/BR#4** | 4.42 | 14.46 | 28.16 | 55.68 |
| **$DF_{Max}$** | 0.82 | 0.74 | 0.65 | 0.66 |

**Table 9: Summary of Magnitude σ Statistics.**

Tables 8 and 9 show a summary of the Magnitude |μ| and σ statistics, respectively. Similar conclusions to those given for the time domain results can be made here. Although it is true that in all cases, the minimum values of columns three through five are larger than the values in column two, the difference is not significant in all cases to reliably identify the defective devices. Notably, the minimum |μ| statistics for all experiments are less than a factor of two larger than the regression line error estimate while the same is true

of the σ statistics for the Open-Drain and Internodal-Bridge experiments.

| \|μ\| | Experiment | | | |
|---|---|---|---|---|
| **Device/Experiment** | **Control** | **Open-Drain** | **Internodal-Bridge** | **Feedback-Bridge** |
| **OD/BR#1** | 2.88 | **248.29** | 66.51 | 15.86 |
| **OD/BR#2** | **3.29** | 272.43 | 77.37 | 25.10 |
| **OD/BR#3** | 1.48 | 327.77 | **60.54** | 38.60 |
| **OD/BR#4** | 2.96 | 306.71 | 94.39 | **15.74** |
| **$DF_{Max}$** | 0.75 | 0.73 | 0.74 | 0.67 |

**Table 10: Summary of Phase |μ| Statistics.**

| σ | Experiment | | | |
|---|---|---|---|---|
| **Device/Experiment** | **Control** | **Open-Drain** | **Internodal-Bridge** | **Feedback-Bridge** |
| **OD/BR#1** | 3.57 | **425.62** | 214.58 | 48.21 |
| **OD/BR#2** | **4.21** | 434.79 | 227.15 | 91.82 |
| **OD/BR#3** | 1.63 | 556.87 | **117.59** | 120.26 |
| **OD/BR#4** | 3.01 | 514.93 | 303.64 | **40.81** |
| **$DF_{Max}$** | 0.18 | 0.80 | 0.76 | 0.68 |

**Table 11: Summary of Phase σ Statistics.**

Tables 10 and 11 show a summary of the Phase |μ| and σ statistics, respectively. It is clear that the phase results are superior to both the time and magnitude results. First, the smallest minimum |μ| statistic, given in column five as 15.74, is nearly a factor of five larger than the regression line error estimate of 3.29 given in column two. The factor increases to nearly ten for σ in Table 11. In either case, the |μ| and σ statistics computed using test sequences that provoke the defect are able to capture the signal variation to a significant degree. This additional tolerance beyond the maximum values given in column two is important, particularly in its relation to the 1 - α confidence limits or process tolerance zone. More specifically, the width of this tolerance zone is directly proportional to the degree of confidence that a positive defect detection decision is correct.

Further evidence that the phase results are superior to the time and magnitude results is obtained by ranking the experiments by the amount of signal variation introduced by each of the defects. A straightforward means of determining this rank is simply to count the number of sensitized paths disrupted by the defect. For example, the test sequence used in the Open-Drain experiment causes faults on three sensitized

paths. The test sequence of the Internodal-Bridging experiment causes faults on two sensitized paths while the test sequence used in the Feedback-Bridging experiment causes a fault on a single sensitized path. Except of a single instance, the ranks of $|\mu|$ and $\sigma$ statistics correspond to this ordering as shown from left to right along each row of columns three through five in Tables 10 and 11. This correspondence is not unexpected since each of the faulted paths contribute to off-path signal variation. Therefore, in addition to providing more significant statistical values, the phase results are consistent with the observed fault behavior across experiments.

The $|\mu|$ and $\sigma$ statistics provide the basis on which a defect detection algorithm can be devised. We recognize that any type of device testing method requires a test vector generation strategy and we discuss the criteria important to TSA in the next section. Given a set of suitable test vector pairs and a set of known defect-free devices, device testing can be carried out in a straightforward manner as follows. The regression lines of pairing between selected test point signals are derived and the $|\mu|$ and $\sigma$ statistics are computed under each of the test sequences. A second set of known defect-free devices are used to evaluate the error in the regression line estimates and the process is repeated until the error is acceptably small. The process tolerance zones based on 1 - $\alpha$ confidence limits are derived under each test sequence. As discussed above, these zones account for variation due to unmodeled variables such as measurement noise and intra-device process tolerance effects. The $|\mu|$ and $\sigma$ statistics of each test device are then computed and compared against the process tolerance zone limits. If a $|\mu|$ or $\sigma$ statistic falls outside of the process tolerance zone under any of the test sequences, the device is marked as defective.

## 7.0 Summary and Conclusions

We presented a statistical technique to identify defects in digital integrated circuits that is based on linear regression analysis of transient signal data. The variations in the transient signals of defect-free and defective devices are captured at multiple test points using Signature Waveforms (SWs). We devised an efficient method of compressing the variation in SWs to a single value called a Trapezoidal Rule Area or TRA. TRAs represent the area under the SW curves computed using a Trapezoidal Rule integration method.

TRAs are advantageous because they are easy to compute and reduce the time and complexity of waveform post-processing. More importantly, however, is the linear property that we have observed in the TRAs across devices affected only by process tolerance effects. We exploit this property in the scatter plots

of test point pairings by computing a regression line through the defect-free data points, as a means of isolating the variations caused by defects. The variations introduced by defects are captured by computing residuals, and summarized for each device in two statistics, $|\mu|$ and $\sigma$, which measure the average deviation and the dispersion of the residuals around the regression lines.

We used the $|\mu|$ and $\sigma$ statistics to evaluate the effectiveness of the time, Fourier magnitude and phase TRAs in capturing variations caused by defects in four hardware experiments. Since the number of test devices in our experiments was small, we estimated the error in the regression lines using a control experiment and found the regression lines to be reasonably estimated. We compared the $|\mu|$ and $\sigma$ statistics of this experiment with those obtained from three defective device experiments and determined that the phase analysis yielded values that were consistently larger than the time domain and magnitude analysis with respect to the regression line estimation error. For example, we measured regression line error for $|\mu|$ that was less than a factor of five times larger than the expected value. However, the smallest $|\mu|$ statistics in the defective device experiments was twenty-three times larger than the expected value. $\sigma$ yielded factors of twenty-four and sixty for these experiments, respectively. Therefore, the phase TRAs provide the highest degree of confidence that a positive defect detection decision is correct.

Based on these experimental results, we proposed an algorithm to automate the detection of defects in TSA. The algorithm is dependent on the $1 - \alpha$ confidence limits or process tolerance zones derived using larger sets of defect-free device sets. Defective devices are identified by comparing the $|\mu|$ and $\sigma$ statistics with the $1 - \alpha$ confidence limits under each test sequence and, for tests in which the former exceeds the latter, the device is marked as defective. Accurate estimates of the $1 - \alpha$ confidence limits are necessary because they account for variation due to unmodeled variables such as measurement noise and intra-device process tolerances.

We are conducting a set of modeling experiments designed to determine the relative contributions of the primary coupling mechanisms, namely the power supply, internodal, well and substrate. A second objective of these experiments is to better understand the relationship between variations in phase and the presence of a defect. The sensitivity of the method to the variations caused by other types of shorting and open defects is also under investigation in these experiments. This information will help us evaluate the scalability of the technique to larger devices by providing the test point number and position requirements necessary in order to attain suitable fault coverage.

We are also evaluating the applicability of TSA to failure analysis in these experiments. Since TSA is based on the analysis of test point signals measured at distinct topological locations on the device, implicit information about the location of the defect is available in the multiple test point waveforms. The variety of defect types that we have introduced into the test devices of these experiments will allow the signal behavior of the defects to be characterized as well.

## Acknowledgments

We would like to acknowledge Professor Philippe Marchand at the University of California San Diego and Professor Hong Koo Kim at the University of Pittsburgh for providing laboratory equipment and facilities for this research.

## References

[1] J. F. Plusquellic. "Digital Integrated Circuit Testing Using Transient Signal Analysis," Ph.D. Dissertation, Department of Computer Science, University of Pittsburgh, August, 1997.

[2] J. F. Plusquellic, D. M. Chiarulli, and S. P. Levitan. "Digital IC device testing by transient signal analysis (TSA)," *Electronics Letters*, 31(18):1568–1570, August 1995.

[3] J. F. Plusquellic, D. M. Chiarulli, and S. P. Levitan. "Digital Integrated Circuit Testing using Transient Signal Analysis," *International Test Conference*, pp. 481-490, October 1996.

[4] J. F. Plusquellic, D. M. Chiarulli, and S. P. Levitan. "Identification of Defective CMOS Devices using Correlation and Regression Analysis of Frequency Domain Transient Signal Data," *International Test Conference*, pp. 40-49, November 1997.

[5] M. W. Levi. CMOS is Most Testable. In *IEEE Test Conference*, pages 217-220, 1981.

[6] F. J. Ferguson, M. Taylor and T. Larrabee. Testing for Parametric Faults in Static CMOS Circuits. In *International Test Conference*, pages 436-443, 1990.

[7] C. F. Hawkins, J. M. Soden, A. W. Righter and J. Ferguson. Defect Classes - An Overdue Paradigm for CMOS IC Testing. In *International Test Conference*, pages 413-425, 1994.

[8] J. M. Soden and C. F. Hawkins. Electrical properties and detection methods for CMOS IC defects. In *Proceeding of the European Test Conference*, pages 159–167, 1989.

[9] A. P. Dorey, B. K. Jones, A. M. D. Richardson, and Y. Z. Xu. *Rapid Reliability Assessment of VLSICs*. Plenum Press, 1990.

[10] T. M. Storey and W. Maly. CMOS bridging fault detection. In *International Test Conference*, pages 1123–1132, 1991.

[11] J. F. Frenzel and P. N. Marinos. Power supply current signature (PSCS) analysis: A new approach to system testing. In *International Test Conference*, pages 125–135, 1987.

[12] E. P. Hsieh, R. A. Rasmussen, L. J. Vidunas, and W. T. Davis. Delay test generation. In *Proceeding of the 14th Design Automation Conference*, pages 486–491, 1977.

[13] C J. Lin and S. M. Reddy. On delay fault testing in logic circuits. *IEEE Transactions on Computer-Aided Design*, CAD-6(5):694–703, September 1987.

[14] S. D. McEuen. $I_{DDQ}$ benefits. In *VLSI Test Symposium*, pages 285–290, 1991.

[15] A. D. Singh, H. Rasheed, and W. W. Weber. $I_{DDQ}$ testing of CMOS opens: An experimental study. In *International Test Conference*, pages 479–489, 1995.

[16] E. McCluskey(Moderator), K. Baker(Organizer), W. Maly, W. Needham, M. Sachdev(Panelists), "Will $I_{DDQ}$ Testing Leak Away in Deep Sub-Micron Technology?", *International Test Conference*, Panel 7, 1996.

[17] M. Hashizume, K. Yamada, T. Tamesada, and M. Kawakami. Fault detection of combinatorial circuits based on supply current. In *International Test Conference*, pages 374–380, 1988.

[18] A. P. Dorey, B. K. Jones, A. M. Richardson, P. C. Russel, and Y. Z. Zu. Reliability testing by precise electrical measurement. In *International Test Conference*, pages 369–373, 1988.

[19] J. S. Beasley, H. Ramamurthy, J. Ramirez-Angulo, and M. DeYong. $I_{DD}$ pulse response testing of analog and digital CMOS circuits. In *International Test Conference*, pages 626–634, 1993.

[20] R. Z. Makki, S. Su, and T. Nagle. Transient power supply current testing of digital CMOS circuits. In *International Test Conference*, pages 892–901, 1995.

[21] A. K. Pramanick and S. M. Reddy. On the detection of delay faults. In *International Test Conference*, pages 845–856, 1988.

[22] A. Pierzynska and S. Pilarski. Non-Robust versus Robust. In *International Test Conference*, pages 123-131, 1995.

[23] E. S. Park, M. R. Mercer, and T. W. Williams. Statistical delay fault coverage and defect level for delay faults. In *International Test Conference*, pages 492–499, 1988.
[24] F. Franco and E. J. McCluskey. Delay testing of digital circuits by output waveform analysis. In *International Test Conference*, pages 798–807, 1991.
[25] A. Chatterjee, R. Jayabharathi, P. Pant and J. A. Abraham. Non-Robust Tests for Stuck-Fault Detection Using Signal Waveform Analysis: Feasibility and Advantages. In *VLSI Test Symposium*, pages 354-359, 1996.
[26] A. Wu, T. Lin, C. Tseng, and J. Meador. Neural network diagnosis of IC faults. In *VLSI Test Symposium*, pages 199–203, 1991.
[27] C. Thibeault. Detection and location of faults and defects using digital signal processing. In *VLSI Test Symposium*, pages 262–267, 1995.
[28] S. C. Ma, P. Franco, and E. J. McCluskey. An experimental chip to evaluate test techniques: Experiment results. In *International Test Conference*, pages 663–672, 1995.
[29] P. C. Maxwell, R. C. Aitken, V. Johansen and I. Chiang. The effectiveness of $I_{DDQ}$, Functional and Scan Tests: How many fault coverages do we need? In *International Test Conference*, pages 168-177, 1992.
[30] C. L. Henderson, J. M. Soden and C. F. Hawkins. The behavior and testing implications of CMOS IC logic gate open circuits. In *International Test Conference*, pages 302-310, 1991
[31] F. Brglez and H. Fujiwara. A neutral netlist of 10 combinational benchmark circuits and a target translator in FORTRAN. *Special Session on ATPG and Fault Simulation, Int. Symposium on Circuits and Systems*, pages 663-698, June 1985.